ELSEVIER

Journal of Structural Geology 28 (2006) 536–543

JOURNAL OF STRUCTURAL GEOLOGY

www.elsevier.com/locate/jsg

Short note: A velocity description of shear fault-bend folding

Stuart Hardy [a,*], Christopher D. Connors [b]

[a] *ICREA (Institució Catalana de Recerca i Estudis Avançats) and GGAC, Departament de Geodinàmica i Geofísica, Facultat de Geologia, Universitat de Barcelona, Catalunya, Spain*

[b] *Department of Geology, Washington and Lee University, Lexington, Virginia, USA*

Received 23 August 2005; received in revised form 19 December 2005; accepted 30 December 2005

Abstract

This short note presents a derivation of the velocity description of deformation for the geometric models of pure-shear and simple-shear fault-bend folding. This allows the calculation of rates of displacement, uplift and limb-rotation associated with such structures and their comparison with classical fault-bend folds. Using this velocity description, we examine the differences between pure-shear and simple-shear fault-bend folds, in terms of uplift, limb rotation and particle trajectories resulting from deformation.

Keywords: Deformation; Kinematics; Fault-bend; Velocities

1. Introduction

The concept that thrust sheets might undergo substantial internal deformation is not new, but its quantification and application to fault-bend folding is (Jordan and Noack, 1992; Suppe et al., 2004). In particular, Suppe et al. (2004) have recently put forward a novel geometric model of 'shear fault-bend folding' that encompasses both simple shear and pure shear in a basal detachment zone, developed as a result of observations that this type of shear is commonly observed in seismic and field examples (see Suppe et al., 2004). Shear fault-bend folding produces ramp anticlines with very distinctive shapes: the anticlines are characterized by long, gently dipping backlimbs that dip less than the fault ramp (Suppe et al., 2004; Fig. 1a and b). A key feature of this model is that the ramp anticline grows by both limb rotation and kink-band migration, leading to backlimb dips and limb lengths that increase progressively with fault slip. Shear fault-bend folding, in the limit of zero basal shear zone thickness, is identical to classical fault-bend folding above a basal detachment where the backlimb dip is equal to the fault dip (Fig. 1c; Suppe, 1983). Suppe et al. (2004) successfully compared the shear fault-bend folding model with some well-constrained natural examples in the Cascadia and Nankai subduction zones, and shear fault-bend folding has been shown to be common in passive-margin toe-thrusts in the Niger Delta (Corredor et al., 2005).

However, while this geometric model appears to match observational data very well, there is no simple analytic method of quantifying rates of uplift and rotation associated with such structures, enabling their combination with models of growth sedimentation or other rate-dependent processes (cf. Hardy et al., 1996). This short note addresses this issue by deriving an equivalent velocity description of deformation from the geometric model of shear fault-bend folding. We illustrate its use by examining the differences between pure-shear and simple-shear fault-bend folds, in terms of uplift, limb rotation and particle trajectories resulting from deformation.

2. Shear fault-bend folding

2.1. Geometric description

It is not the intention of this section to give a detailed derivation of the geometric model of shear fault-bend folding but rather to provide sufficient background to show the manner in which it can be transformed into a velocity description of deformation. For a detailed description of shear fault-bend folding the interested reader is referred to Suppe et al. (2004). Shear fault-bend folding fundamentally derives from the premise that distributed deformation may occur within a weak décollement of finite thickness at the base of a fault ramp (Fig. 1). Deformation in this unit is distinct from that in the

* Corresponding author
E-mail addresses: stuart.hardy@icrea.es (S. Hardy), ConnorsC@wlu.edu (C.D. Connors).

0191-8141/$ - see front matter © 2006 Elsevier Ltd. All rights reserved.
doi:10.1016/j.jsg.2005.12.015

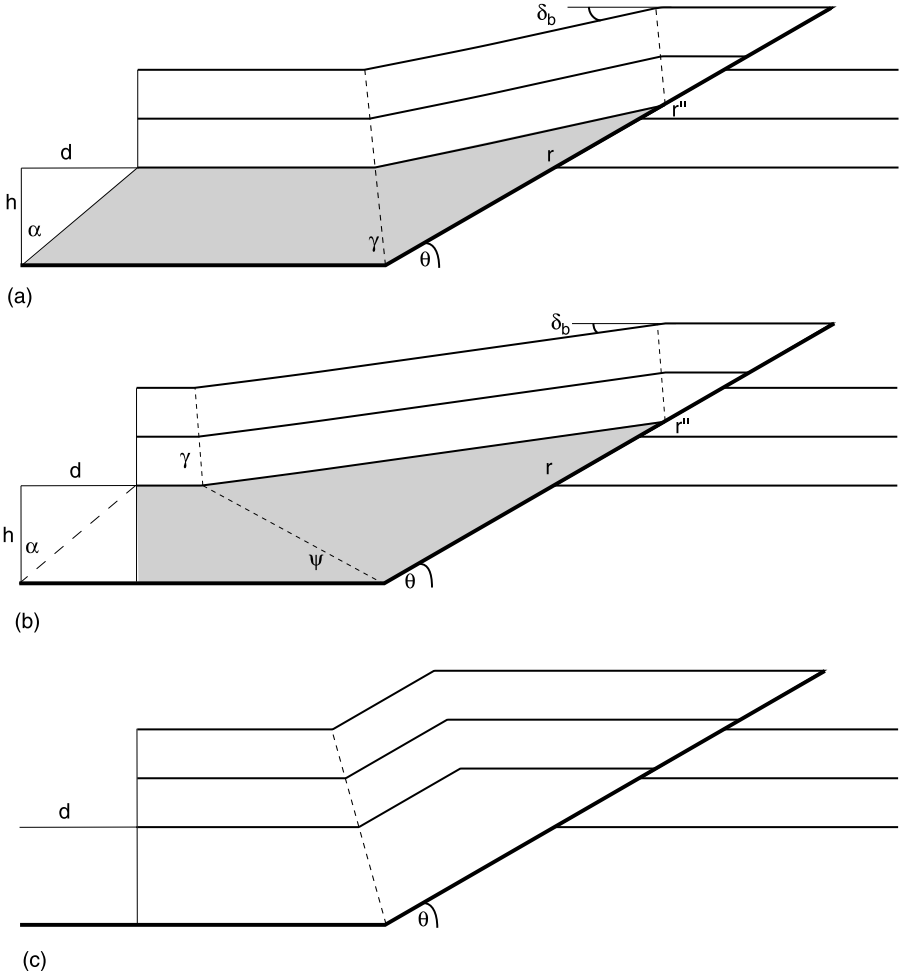

Fig. 1. The geometric models of (a) simple-shear fault-bend folding and (b) pure-shear fault-bend folding, where α is shear or dimensionless fault slip ($\tan^{-1}(d/h)$), δ_b is backlimb dip, θ is ramp dip, γ is the angle of the synclinal axial surface and ψ is its offset in the case of pure-shear fault-bend folding. Basal décollement zone illustrated in grey. In these examples we show a fold developing above a 30° ramp, with a 500-m-thick basal décollement zone and 600 m displacement. (c) Equivalent classical fault-bend fold with a 30° ramp and 600 m displacement. See text for discussion.

overlying strata, which are the particular focus of this paper. There are two end-members: pure-shear and simple-shear fault-bend folding. In simple-shear fault-bend folding, the décollement layer undergoes bedding-parallel simple shear with no actual basal fault-slip per se (Fig. 1a). In pure-shear fault-bend folding, the basal layer undergoes shortening parallel to bedding (Fig. 1b). In both end-members the weak layer is overlain by strata that undergo flexural slip and have no external shear applied, conserving layer thickness and bed length. The fundamental equation of shear fault-bend folding is as follows (Suppe et al., 2004; Fig. 1):

$$\cot(\alpha) = \frac{\sin\delta_b}{2C}\left[\left[\frac{1}{\sin\delta_b\cot\theta + 1 - \cos\delta_b}\right]^2 - \left[\frac{1}{\sin\delta_b\cot\theta + 1 - \cos\delta_b}\right]\right] \quad (1)$$

where $\alpha = \tan^{-1}(d/h)$ is an external shear or a dimensionless ratio of displacement to basal thickness, δ_b is backlimb dip, θ is ramp dip and C is a constant representing the ratio of area of shortening to displacement and basal thickness. For the end-member cases, C is 1 for pure-shear and 1/2 for homogeneous simple-shear. In addition, fault-parallel displacement (rr'') is given by (Suppe et al., 2004):

$$rr'' = \frac{d\sin\gamma}{\cos((\delta_b/2) - \theta)} \quad (2)$$

The position and orientation of the back synclinal axial surface is straightforward in the simple-shear case as it bisects all layers:

$$\gamma = 90 - \delta_b/2 \quad (3a)$$

but its angular offset (ψ) within the basal layer in the pure-shear case is given by:

$$\cot\psi = \cot\theta + 2\cot\gamma \quad (3b)$$

Suppe et al. (2004) presented a detailed analysis of this model and showed its application to a variety of natural examples. Below we now derive an equivalent velocity description of deformation of this geometric model and discuss its implications.

2.2. Velocity description

The motivation behind deriving a velocity description of deformation of shear fault-bend folding is to allow us, for an increment of slip, to calculate rates of displacement, uplift and limb-rotation associated with such structures. In shear fault-bend folding two distinct processes are occurring at the same time (for an infinitely small time-step/increment of slip): kink-band migration and limb-rotation. The velocity descriptions of deformation for both of these processes acting on their own already exist (Hardy and Poblet, 1994, 1995; Hardy, 1995). A velocity description of deformation for shear fault-bend folding will allow us to separate and to quantify the influence of each process on uplift and rotation rates above such structures.

We present here a velocity description of deformation for shear fault-bend folding solely for material above the basal unit; we do not consider velocities within the basal unit. In order to derive the velocity description we must firstly numerically solve the fundamental equation of shear fault-bend folding, Eq. (1), by Newton's method, as there is no analytic solution. This is done by re-arranging Eq. (1) such that δ_b occurs on both the left- and right-hand sides of the equation. We then choose an approximate solution for the backlimb dip, δ_b, solve Eq. (1) for δ_b, and then use the derived value of this variable as the new guess until both guess and solution are (to some specified degree) equivalent. This allows us to derive, for a given ramp dip and shear ($\tan^{-1}(d/h)$), the backlimb dip, δ_b. It is then straightforward to calculate, for an increment of slip, the limb rotation rate ω (radians per time-step), which is given as the time derivative of the change in limb dip over that time-step. We then solve for the position of the upper axial surface by finding the distance rr'' from Eq. (2), and the position and orientation of the synclinal axial surface using Eq. (3a). Therefore, for a finite time-step, and increment of fault slip, we now know the position of all the axial surfaces that define the boundaries of the different domains in the growing fold (Fig. 2). Velocities can now be derived for each of these domains. It is important to note that there are three distinct velocity domains above the basal décollement layer. In domain 1, material is simply being displaced parallel to the basal décollement, in domain 2, material is both rotating and being displaced parallel to the current orientation of the backlimb, while in domain 3, material moves at the same rate as the upper limit of domain 2, ensuring both continuity and no gaps/overlaps with the fault. The horizontal and vertical velocities within the three domains are then given by:Domain 1:

$$u = s \qquad v = 0 \tag{4}$$

Domain 2:

$$u = s.\cos(\delta_b) - \omega(y - y_0) \qquad v = s.\sin(\delta_b) + \omega(x - x_0) \tag{5}$$

Domain 3:

$$u = u_b \qquad v = v_b \tag{6}$$

where u and v are horizontal and vertical velocities (m/ka), respectively, s is the slip rate (m/ka), ω is the rotation rate, x and y are the horizontal and vertical locations of a point, x_0 and y_0 are coordinates of the centre of rotation for that point (the point of intersection between the kink axis and the bedding surface that contains that point), and u_b and v_b are the velocities (m/ka) at the boundary of domains 2 and 3. We present a more general version of this analysis for the case of a ramp that connects to an upper fault flat in a later section.

These domains and their velocities are valid for both simple- and pure-shear fault-bend folds. Importantly, for domain 2, they explicitly separate the influence of kink-band migration and limb-rotation on the horizontal and vertical motion above such structures. In the limit of zero basal shear zone thickness, the backlimb undergoes instantaneous rotation and the velocities are identical to those of classical fault-bend folding (cf. Hardy and Poblet, 1995). Having derived this velocity description of shear fault-bend folding, we can now proceed to examine the evolution of, and uplift and rotation above, such folds and compare them with classical fault-bend folds.

3. Progressive evolution of a shear fault-bend fold with growth strata

In this section we show the equivalence to the geometric model of our velocity-based approach to shear fault-bend

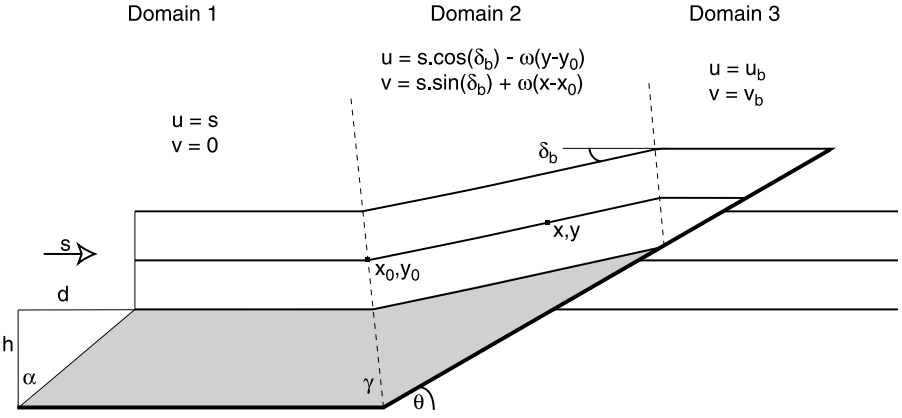

Fig. 2. The velocity model of shear fault-bend folding illustrated for the simple-shear case: u and v are horizontal and vertical velocities, respectively, s is the slip rate, ω is the rotation rate, x and y are the horizontal and vertical locations of a point, x_0 and y_0 are coordinates of the centre of rotation for that point and u_b and v_b are the velocities at the boundary of domains 2 and 3. The basal unit has a thickness of h and a displacement of d. See text for discussion.

folding by showing the progressive evolution of a simple-shear fault-bend fold. We examine the evolution of a simple-shear fault-bend fold developing above a 30° ramp, with a 500-m-thick basal décollement zone. Far-field fault slip is assumed to be 1.0 m/ka and the model is run for 600 ka, giving 600 m displacement. In addition we include simple 'fill to the top' growth sedimentation beneath a base-level that rises at 0.75 m/ka, growth strata are added every 100 ka. We numerically model this using a simple Lagrangian coordinate system, with a spatial resolution of 7.5 m and a time-step of 100 yrs.

The evolution of this structure after 0, 100, 200, 400 and 600 m displacement is shown in Fig. 3. We see clearly from this figure the manner in which the fold develops: the limb lengthens with increasing displacement and rotates at the same time. The growth strata reflect these kinematics showing components of both limb rotation (a fanning wedge of strata) and a growth triangle reflecting kink-band migration. We have quantitatively confirmed that our velocity description of deformation is equivalent to the theoretical geometric model in terms of limb dips, lengths and growth patterns.

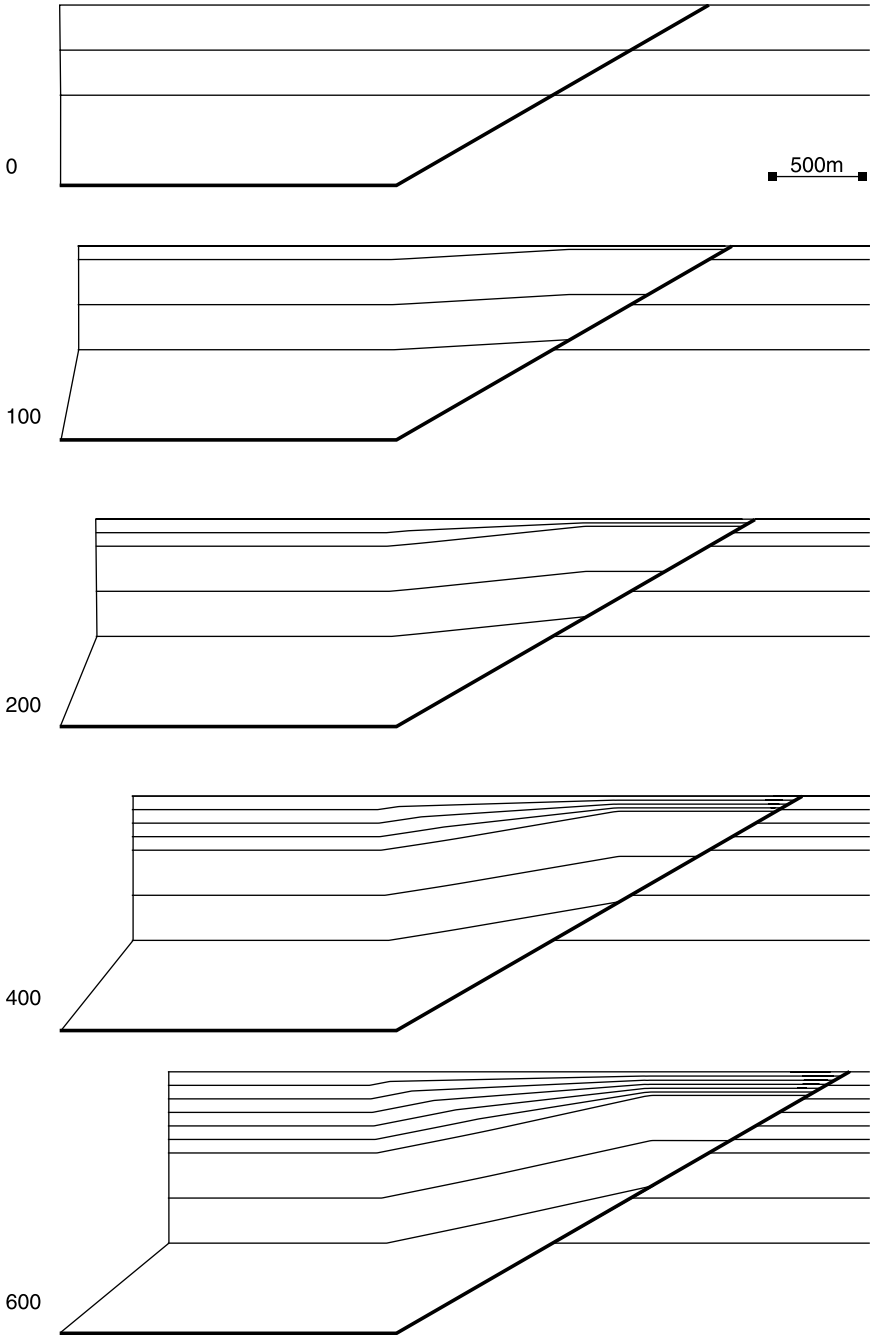

Fig. 3. Evolution of a simple-shear fault-bend fold developing above a 30° ramp, with a 500-m-thick basal décollement zone. Far field fault slip is assumed to be 1.0 m/ka and the model is run for 600 ka, giving 600 m displacement. We include simple 'fill to the top' growth sedimentation beneath a base-level, which rises at 0.75 m/ka; growth strata are added every 100 ka. Model is shown at 0, 100, 200, 400 and 600 m displacement.

4. Uplift and rotation above shear fault-bend folds

One aspect of shear fault-bend folding that can immediately be derived from a velocity description of deformation is the manner in which uplift of the fold crest and rotation of the fold limb occurs as displacement is accumulated. We illustrate this in Fig. 4 for a simple-shear and a pure-shear fault-bend fold developed under identical conditions. As above, both folds develop above a 30° ramp, with a 500-m-thick basal décollement zone and 600 m displacement. Far-field fault slip is set at 1.0 m/ka.

The geometries of the final folds are shown in Fig. 1a and b. The uplift of both fold crests with time is shown in Fig. 4a and the corresponding rates of uplift are shown in Fig. 4b. In both cases we see that the difference in absolute uplift between a pure-shear and a simple-shear fault-bend fold is negligible, with the pure-shear case having marginally more uplift. On Fig. 4a we also show the theoretical uplift above a classical fault-bend fold developing under identical conditions. It is clear that both simple-shear and pure-shear fault-bend folds produce more uplift than their classical counterparts. We have confirmed that this is a general feature of shear fault-bend folding (Fig. 5).

It can also be seen that, for both folds, the rate of uplift decreases as displacement is accumulated, approaching a value of 0.50 m/ka consistent with the convergence of classical fault-bend folding and shear fault-bend folding kinematics for very large displacements or small shear zone thickness (Fig. 4b). The evolution of limb dip with time for both folds is shown in Fig. 4c. It can be seen that there are much more marked differences in backlimb dip between the end-member models, with the pure-shear fold having a gentler backlimb. In addition, in both cases we see that rotation rate decreases markedly as displacement accrues (Fig. 4d). This is particularly so in the case of simple-shear fault-bend folding.

These uplift and rotation rates, and their temporal and spatial variations, are quite distinctive. Importantly, in a manner similar to other styles of fault-related folding (cf. Hardy and Poblet, 2005), they offer the possibility that, with appropriate geomorphic or neotectonic data, the kinematics and, ultimately, deeper structure of an active fold may be better constrained. An obvious important difference between shear and classical fault-bend folding in this regard is in the inferred far-field slip rates based on limb dip and uplift rates. For active structures suspected to be fault-bend folds, it is common to calculate (slip rate) = (uplift rate)/sin(limb dip), e.g. Lavé and Avouac (2000). Implicit in this calculation is that the thrust is stepping up from a detachment and that it is a classical fault-bend fold, i.e. $\delta_b = \theta$. Fig. 5 shows that if a structure is a shear fault-bend fold this approach always underestimates the slip rate. For example, for a measured limb dip = 20° with a ramp dip = 30°, the slip rate is underestimated by approximately 63%.

5. Particle trajectories in a shear fault-bend fold

In order to illustrate the key differences between shear fault-bend folding and classical fault-bend folding it is useful to examine particle trajectories above the fault ramp in the models discussed here. These particle trajectories are illustrated in

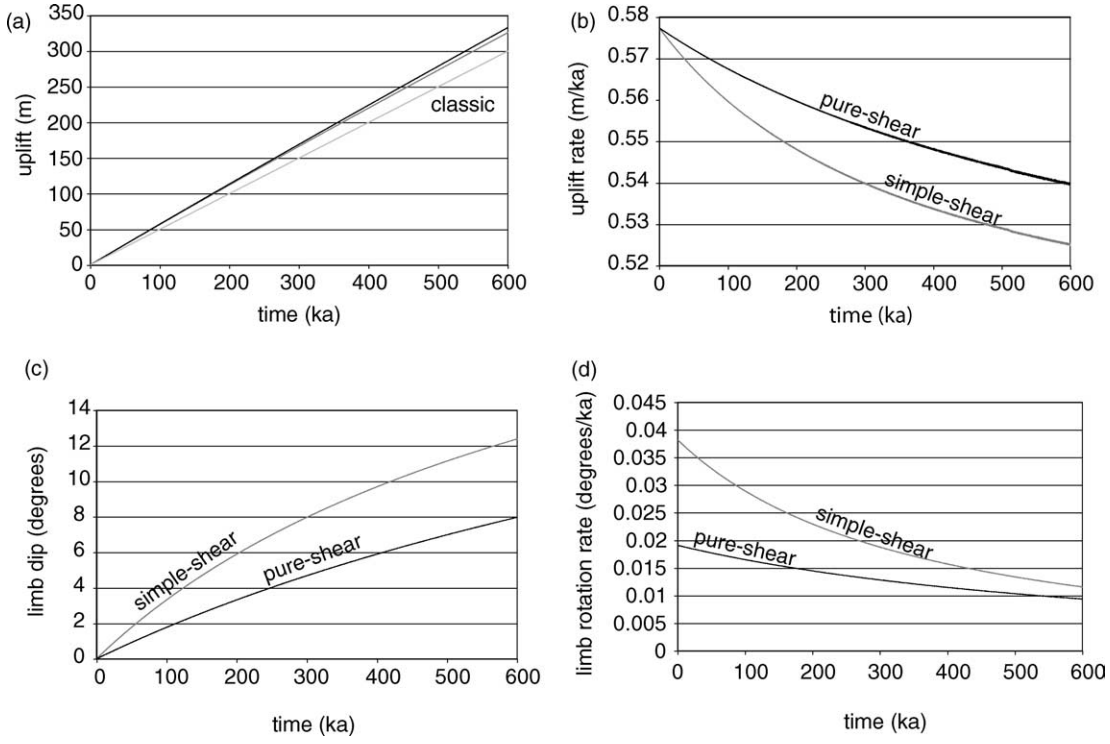

Fig. 4. Folds developed after 600 m displacement above a basal zone 500 m thick, with a ramp of 30° and a far-field slip of 1 m/ka. (a) Uplift (m) and (b) uplift rate (m/ka) above the fold crest vs. time, (c) limb dip (°) and (d) limb rotation rate (°/ka) vs. time (for final geometry, see Fig. 1a–c).

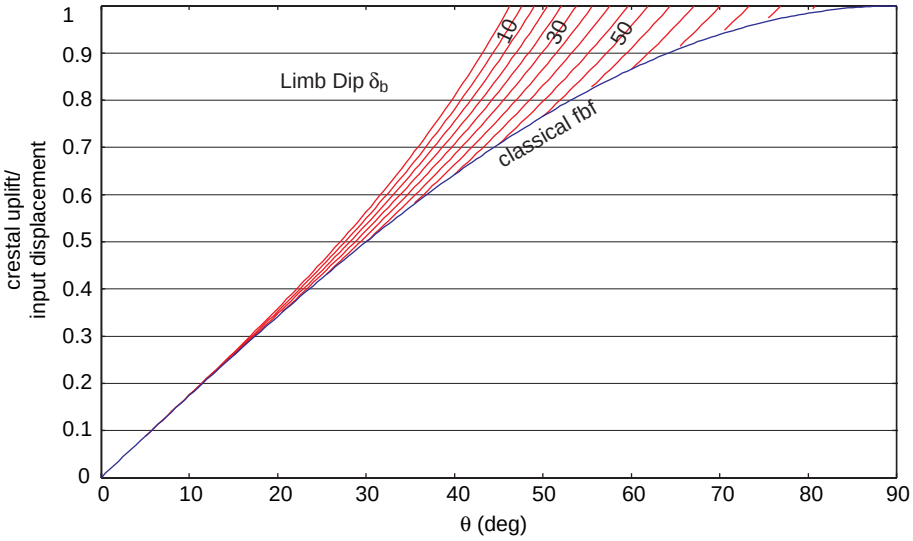

Fig. 5. Relationship of fault ramp, θ, vs. uplift for shear fault-bend folds of varying limb dip, δ_b. Uplift has been normalized by the input displacement parallel to the décollement. This ratio can be equivalently thought of as the uplift rate to far-field slip rate for active structures.

Fig. 6, for a subset of modelled particles, for simple-shear, pure-shear and classical fault-bend folding.

In general, for both simple-shear (Fig. 6a) and pure-shear (Fig. 6b) fault-bend folding the particle trajectories are complex and curvilinear reflecting the kinematics in the fold limb, which combines both kink-band migration and limb rotation. As one progresses away from the crest of the fold along each of the three marker beds there is a transition from

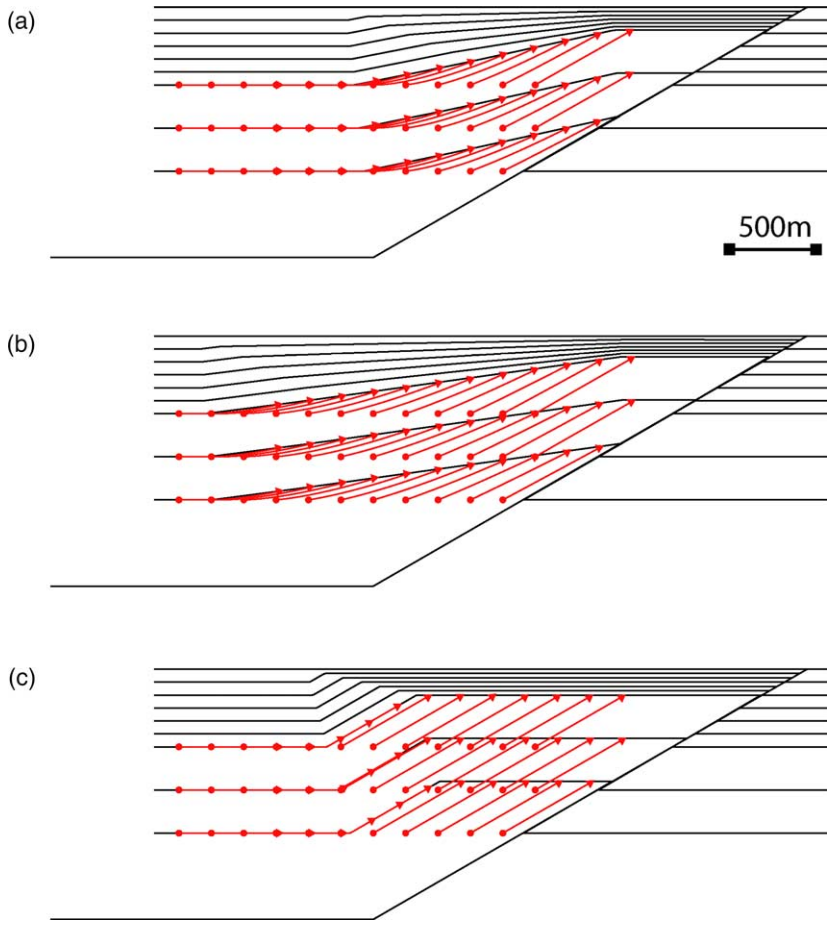

Fig. 6. Particle trajectories above the fault ramp, for a subset of particles, in the models discussed above: (a) simple-shear, (b) pure-shear and (c) classical fault-bend folding.

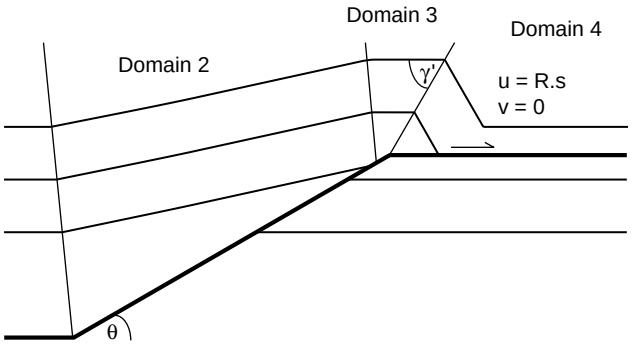

Fig. 7. Illustration of the additional velocity domain needed in the kinematic model when the ramp associated with a shear fault-bend fold connects to an upper flat. Domains 1–3 are as in Fig. 3, whereas domain 4 contains only a simple translational component of motion; see text for discussion.

trajectories sub-parallel to the fault ramp to trajectories sub-parallel to the décollement. This is because the axis of rotation is the intersection of a layer and the synclinal axial surface and with time, particles are moving farther from this axis of rotation. Particles that are farther from the synclinal axial surface have a greater component of displacement due to rotation than those close to the axis of rotation and thus have a greater vertical component. In contrast, the particle trajectories for a classical fault-bend fold (Fig. 6c) are markedly different. They are all parallel to the fault and only change orientation (instantaneously) across the synclinal axial surface. This kink-band migration component can also be seen in the shear fault-bend fold trajectories as an abrupt change in orientation at the synclinal axial surface. The geometry of the corresponding growth strata reflects this variation in kinematics.

6. Shear fault-bend folds with an upper flat

In the main body of this paper we have derived a velocity description of deformation based on the geometric model originally presented by Suppe et al. (2004). Here we present a slight generalization of the method to include an upper flat in the kinematic scheme. This introduces a fourth velocity domain into the kinematic description (Fig. 7); the three other domains are identical to those previously described. We assume that, unlike our previous derivation, the ramp links with an upper flat (Fig. 7). The kinematics describing the transition from the flat crest of the structure to the dipping forelimb are extremely simple and are governed by the equations of Suppe (1983). The inclination of the frontlimb axial surface (γ') and the change in slip across it (R) are given by:

$$\tan(\theta) = \sin(2\gamma')/(2\cos^2\gamma' + 1) \tag{7}$$

$$R = \sin(\gamma' - \theta)/\sin(\gamma') \tag{8}$$

Thus, given the slip rate parallel to the fault in domain 3 (s) and the orientation of the frontlimb axial surface, the horizontal and vertical velocities in domain 4 are:

$$u = R.s \qquad v = 0 \tag{9}$$

Therefore in domain 4 there is only translation parallel to the upper flat and thus the vertical velocity is zero. Once calculated, it is a simple matter to include this additional velocity domain in the modelling scheme. We show this in Fig. 8 where both simple-shear and pure-shear fault-bend folds with boundary conditions identical to those illustrated previously, but with an upper flat and including growth strata,

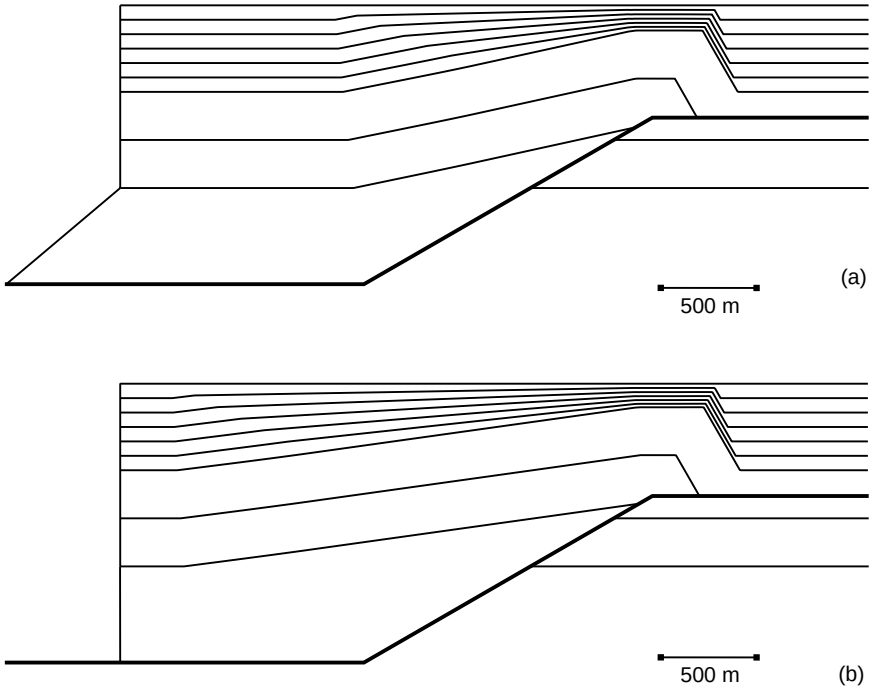

Fig. 8. Evolution of a (a) simple-shear and (b) pure-shear fault-bend fold developed above a 30° ramp, which connects to an upper flat, with a 500-m-thick basal décollement zone. Far field fault slip is assumed to be 1.0 m/ka and the model is run for 600 ka, giving 600 m displacement. We include simple 'fill to the top' growth sedimentation beneath a base-level, which rises at 0.75 m/ka; growth strata are added every 100 ka.

are shown. What is clear is that in both cases the displacement on the upper ramp is small compared with the far-field slip.

7. Discussion and conclusions

This short note has derived a velocity description of shear fault-bend folding for both simple- and pure-shear end-members. The power of this approach is that it is consistent with the geometric model but allows rates of uplift and rotation to be derived given an external slip rate. The derived velocities can then be used in simple mathematical models to test the geometric consequences of such kinematics on a variety of different growth sediment scenarios, or other rate-dependent processes. The inverse problem, determining rates of fault slip, can also be approached if appropriate geometric and age constraints are available for a given structure.

In this paper it has not been our intention to promote or refute a particular model of fault-related folding, or to claim that the model examined here is more important or timely than others, but rather to provide a quantification of a particular model in order that its implications may be more fully explored and tested. It complements other recent papers on the kinematics of fault-related folding (fault-bend, fault-propagation or detachment) in which velocity descriptions of deformation have been presented (Hardy and Poblet, 1994, 1995, 2005; Zehnder and Allmendinger, 2000). The differences between some of these end-member models may seem subtle, but the quantification of their kinematics allows, with appropriate data, their distinction.

Finally, while we have examined the nature of deformation within the 'cover' sequence, we have not dealt with deformation within the basal unit, or what happens when the décollement layer is displaced farther than the upper corner of the footwall ramp and folded over the upper footwall flat. In addition our models of sedimentation are very simplistic and do not take into account erosion, transport and sedimentation induced by the growth of a structure. These and other issues are the subject of ongoing research.

Acknowledgements

This short paper grew out of discussions during the international conference on theory and application of fault-related folding held in Beijing, June 2005. The authors are grateful to the conference organizers for hosting such a stimulating meeting and for providing financial support to attend. We would also like to thank reviewers Juohai Jin, Rick Allmendinger and an anonymous reviewer whose comments have helped to greatly improve this manuscript.

References

Corredor, F., Shaw, J.H., Bilotti, F., 2005. Structural styles in the deep-water fold and thrust belts of the Niger Delta. American Association of Petroleum Geologists Bulletin 89, 753–780.

Hardy, S., 1995. A method for quantifying the kinematics of fault-bend folding. Journal of Structural Geology 17 (12), 1785–1788.

Hardy, S., Poblet, J., 1994. Geometric and numerical model of progressive limb rotation in detachment folds. Geology 22, 371–374.

Hardy, S., Poblet, J., 1995. The velocity description of deformation. Paper 2: sediment geometries associated with fault-bend and fault-propagation folds. Marine and Petroleum Geology 12, 165–176.

Hardy, S., Poblet, J., 2005. A method for relating fault geometry, slip rate and uplift data above fault-propagation folds. Basin Research 17, 417–424.

Hardy, S., Poblet, J., McClay, K., Waltham, D., 1996. Mathematical modelling of growth strata associated with fault-related fold structures. In: Buchanan, P.G., Nieuwland, D.A. (Eds.), Modern Developments in Structural Interpretation, Validation and Modelling Geological Society of London Special Publication 99, pp. 265–282.

Jordan, P., Noack, T., 1992. Hanging wall geometry of overthrusts emanating from ductile decollements. In: McClay, K.R. (Ed.), Thrust Tectonics. Chapman & Hall, London, pp. 311–318.

Lavé, J., Avouac, J.P., 2000. Active folding of fluvial terraces across the Siwaliks Hills, Himalayas of central Nepal. Journal of Geophysical Research 105, 5735–5770.

Suppe, J., 1983. Geometry and kinematics of fault-bend folding. American Journal of Science 283, 684–721.

Suppe, J., Connors, C.D., Zhang, Y., 2004. Shear fault-bend folding. In: McClay, K.R. (Ed.), Thrust Tectonics and Hydrocarbon Systems AAPG Memoir 82, pp. 303–323.

Zehnder, A.T., Allmendinger, R.W., 2000. Velocity field for the trishear model. Journal of Structural Geology 22, 1009–1014.